# Photon-Mediated Spin-Exchange Dynamics of Spin-1 Atoms: Supplemental Material

(Dated: December 15, 2018)

In this supplement, we elaborate on derivations of theoretical models in the main paper and on details from the experimental sequence. In Sec. I, we derive the spin-exchange Hamiltonian, elaborate on the mean-field model of the spin dynamics, and describe how to relate the strength of the interaction $\chi$ to parameters measured in the experiment. Additionally, we derive the short-time behavior for the spin-mixing Hamiltonian. In Sec. II, we elaborate on the experimental methods and describe the calibration of the vector light shift $\Omega(x)$ by Ramsey spectroscopy.

## I. THEORETICAL BACKGROUND

### A. Derivation of Spin-Exchange Hamiltonian

We here derive the spin-exchange Hamiltonian arising in a driven optical cavity with a magnetic field $\mathbf{B}$ perpendicular to the cavity axis. We consider atoms with hyperfine spin $\mathbf{f}$ and let $\mathbf{B}$ define the quantization axis for the spins, so that $f_i^z$ denotes the spin projection of the $i^{\text{th}}$ atom along the magnetic field. The spins couple to the cavity mode via the Faraday effect [1, 2], which is most conveniently described by defining the Stokes vector $\mathbf{S}$ of the intracavity light. For the light, we choose the *cavity axis* as the quantization axis, defining

$$S_z = \left(a_+^\dagger a_+ - a_-^\dagger a_-\right)/2, \tag{S1}$$

where $a_\pm$ are the annihilation operators for $\sigma_\pm$-polarized cavity modes. The Faraday interaction then takes the form

$$H_I = \Omega S_z \mathcal{F}_x, \tag{S2}$$

where $\mathcal{F} = \sum_i \xi_i \mathbf{f}_i$ denotes the collective spin of the ensemble, weighted according to factors $\Omega\xi_i = g_i^2/\Delta_i$ that account for any inhomogeneity in the vacuum Rabi frequency $g_i$, or of the atomic transition frequency $\omega_i = \omega_c^N - \Delta_i$, where $\omega_c^N$ denotes the cavity mode frequency in the presence of $N$ atoms. The Faraday interaction generates a rotation in the cavity mode polarization by an angle proportional to the 'magnetic field' produced by the atoms along $\mathcal{F}_x$.

The microscopic mechanism for the flip-flop dynamics is more evident if we rewrite the Faraday interaction in terms of operators $\mathcal{H}, \mathcal{V}$ representing the two orthogonal linearly polarized cavity modes:

$$\mathcal{H} = \frac{a_+ + a_-}{\sqrt{2}} \tag{S3}$$

$$\mathcal{V} = \frac{a_+ - a_-}{i\sqrt{2}}. \tag{S4}$$

In terms of the linearly polarized modes, the Stokes vector has $z$-component

$$S_z = \frac{\mathcal{V}^\dagger\mathcal{H} - \mathcal{H}^\dagger\mathcal{V}}{2i}, \tag{S5}$$

yielding an interaction Hamiltonian

$$H_I = \frac{\Omega}{4i}\left(\mathcal{V}^\dagger\mathcal{H} - \mathcal{H}^\dagger\mathcal{V}\right)\left(\mathcal{F}_+ + \mathcal{F}_-\right). \tag{S6}$$

Thus, $H_I$ describes processes wherein an atom flips its spin and transfers a photon between the two linearly polarized cavity modes. These Raman processes are resonant when the drive field is tuned to a frequency $\omega_c^N \pm \omega_Z$. More generally, tuning the drive field to a frequency $\omega_d = \omega_c^N + \delta_c$ results in detunings $\delta_\pm \equiv \delta_c \mp \omega_Z$ from the two Raman resonances.

The dynamics in the driven cavity are described by a master equation with a Hamiltonian of the form

$$H = H_I + \omega_Z F_z + \sum_\pm \left[\omega_c a_\pm^\dagger a_\pm + \varepsilon_\pm e^{-i\omega_d t} a_\pm^\dagger + \varepsilon_\pm^* e^{i\omega_d t} a_\pm\right], \tag{S7}$$

where $\mathbf{F} = \sum_i \mathbf{f}_i$ denotes the uniformly weighted collective spin that couples to the magnetic field and $\varepsilon_\pm$ describe coherent fields driving the cavity on the $\sigma_\pm$ polarized cavity modes. We will analyze the time evolution in an interaction picture wherein states evolve with the trivial portion of the Hamiltonian,

$$H_0 = \omega_Z F_z + \sum_\pm \left[\omega_c a_\pm^\dagger a_\pm\right]. \tag{S8}$$

The remaining dynamics, encoded in the operators, are governed by an effective Hamiltonian $\tilde{H} = UHU^\dagger - H_0$, where $U = e^{-iH_0 t}$. This transformation yields

$$\tilde{H} = \tilde{H}_I + \tilde{H}_{\text{drive}}, \tag{S9}$$

where

$$\tilde{H}_I = \frac{\Omega}{4i}\left(\mathcal{V}^\dagger\mathcal{H} - \mathcal{H}^\dagger\mathcal{V}\right)\left(\mathcal{F}_+ e^{i\omega_Z t} + \mathcal{F}_- e^{-i\omega_Z t}\right), \tag{S10}$$

and

$$\tilde{H}_{\text{drive}} = \sum_\pm \varepsilon_\pm e^{-i\delta_c t} a_\pm^\dagger + \text{h.c.}. \tag{S11}$$

We will henceforth remain in the interaction picture and drop the tilde for notational simplicity.

If we include cavity decay in the model, the time evolution of each operator $\mathcal{O}$ is described by a master equation in Lindblad form,

$$\dot{\mathcal{O}} = i[H, \mathcal{O}] + \frac{\kappa}{2}\sum_\pm \left([a_\pm^\dagger, \mathcal{O}]a_\pm + a_\pm^\dagger[\mathcal{O}, a_\pm]\right). \tag{S12}$$

In the absence of atoms, the cavity field operators thus evolve as

$$\dot{a}_\pm = -\frac{\kappa}{2}a_\pm - i\varepsilon_\pm e^{-i\delta_c t}. \tag{S13}$$

The steady-state field is given by

$$\overline{a}_\pm(t) = \frac{-i\varepsilon_\pm e^{-i\delta_c t}}{\kappa/2 - i\delta_c}. \tag{S14}$$

We will focus on the case of a cavity mode driven with horizontally polarized light, such that the steady-state fields in the linear basis (Eqs. S3-S4) are $\overline{\mathcal{V}} = 0$ and

$$\overline{\mathcal{H}} = \frac{-i\varepsilon e^{-i\delta_c t}}{\kappa/2 - i\delta_c}, \tag{S15}$$

where $\varepsilon = (\varepsilon_+ + \varepsilon_-)/\sqrt{2}$. Then the average number of photons in the driven cavity mode is

$$\overline{n} \equiv |\overline{\mathcal{H}}|^2 = \frac{|\varepsilon|^2}{\delta_c^2 + (\kappa/2)^2}. \tag{S16}$$

It will be useful to write the field operators in terms of the $c$-numbers $\overline{\mathcal{H}}$ and $\overline{\mathcal{V}}$ and the fluctuations $\hat{h}, \hat{v}$ about these values:

$$\hat{\mathcal{H}} = \overline{\mathcal{H}} + \hat{h}, \tag{S17}$$

$$\hat{\mathcal{V}} = \overline{\mathcal{V}} + \hat{v}, \tag{S18}$$

where we have temporarily written explicit hats to emphasize which symbols are operators.

For small fluctuations about the steady-state field values, we can solve for the spin dynamics by including only terms to lowest order in $\hat{h}$ and $\hat{v}$ in the interaction Hamiltonian. The atom-light interaction can thus be approximated as

$$H_I \approx \frac{\Omega/4}{\sqrt{\delta_c^2 + (\kappa/2)^2}}\left(\varepsilon e^{-i\delta_c t - i\phi} v^\dagger + \varepsilon^* e^{i\delta_c t + i\phi} v\right)\left(\mathcal{F}_+ e^{i\omega_Z t} + \mathcal{F}_- e^{-i\omega_Z t}\right). \tag{S19}$$

where $\phi$ is an unimportant phase factor that accounts for the phase delay between the drive field and the cavity field. Here, we can see that resonant spin-flip processes occur only for a laser detuned from cavity resonance by $\delta_c = \pm\omega_Z$. However, for arbitrary drive frequency $\delta_c = \pm\omega_Z + \delta_\pm$, resonant *pairwise* flip-flops can arise from $H_I$ in second-order perturbation theory. To further analyze the spin dynamics, we will adiabatically eliminate the $\hat{v}$ cavity mode by assuming a weak drive $\varepsilon$ and large detuning $\delta_\pm$ from Raman resonance.

By adiabatically eliminating the cavity modes [3], we arrive at an effective Hamiltonian

$$H_{\text{eff}} = \frac{|\Omega\varepsilon/4|^2}{\delta_c^2 + (\kappa/2)^2} \sum_\pm \left( \frac{\delta_\pm}{\delta_\pm^2 + (\kappa/2)^2} \mathcal{F}_\pm \mathcal{F}_\mp \right). \tag{S20}$$

The effective Hamiltonian can be written in the form

$$H_{\text{eff}} = \sum_{i,j} \chi_{ij} \left( f_i^x f_j^x + f_i^y f_j^y \right) + \sum_i h_i f_i^z \tag{S21a}$$

with the coupling constants $\chi_{ij} = \chi_{ij}^+ + \chi_{ij}^-$ given by

$$\chi_{ij}^\pm = \overline{n} \frac{\Omega_i \Omega_j}{16} \frac{\delta_\pm}{\delta_\pm^2 + (\kappa/2)^2}. \tag{S21b}$$

Here, $\Omega_i = \Omega\xi_i$ represents the vector light shift imparted by a circularly polarized intracavity photon to the $i^{\text{th}}$ atom. The extra 'magnetic field' term is generated by commutators of $f_i^x, f_i^y$, and has the form:

$$h_i = \overline{n} \frac{\Omega_i^2}{16} \sum_\pm \frac{(\pm 1)\delta_\pm}{\delta_\pm^2 + (\kappa/2)^2}. \tag{S21c}$$

In the case of uniform coupling, we can ignore this longitudinal field in the dynamics by going into a rotating frame. More generally, this term contributes some dephasing between spins at different positions in the cloud.

The Hamiltonian dynamics are generically accompanied by dissipation described by an effective Lindblad operator

$$L_v = \frac{\Omega\varepsilon}{4} \frac{\sqrt{\kappa}}{\delta_c - i\kappa/2} \sum_\pm \frac{\mathcal{F}_\pm e^{-i\delta_\pm t - i\phi}}{\delta_\pm + i\kappa/2}. \tag{S22}$$

The Lindblad operator consists of two terms that rotate rapidly with respect to one another. We can therefore break these two terms up into separate Lindblad operators:

$$L_\pm = \sqrt{\gamma_\pm} \mathcal{F}_\pm, \tag{S23a}$$

where

$$\gamma_\pm = \overline{n} \frac{\Omega^2}{16} \frac{\kappa}{\delta_\pm^2 + (\kappa/2)^2} \tag{S23b}$$

and we have eliminated phase factors that are irrelevant to the dynamics. Comparing equations S21b and S23b, we see that the interaction-to-decay ratio

$$\frac{\chi_{ij}^\pm}{\gamma_\pm} = \frac{\delta_\pm}{\kappa} \xi_i \xi_j \tag{S24}$$

improves with increasing detuning $\delta_\pm$ from Raman resonance.

### B. Dynamics Including the Light Field

Even in the regime where the adiabatic elimination is not valid, we can write down a full set of Heisenberg equations of motion including the cavity field operators as well as the spin operators. In particular, from the master equation

(Eq. S12) for the Hamiltonian in Eq. S7 with $\mathcal{H}$-polarized drive field, the Heisenberg equations are

$$\dot{\mathcal{V}} = -\Omega \mathcal{F}^x \mathcal{H}/2 - \left(\frac{\kappa}{2} - i\delta_c\right)\mathcal{V} \tag{S25a}$$

$$\dot{\mathcal{H}} = \Omega \mathcal{F}^x \mathcal{V}/2 - \left(\frac{\kappa}{2} - i\delta_c\right)\mathcal{H} - \varepsilon \tag{S25b}$$

$$\dot{f}_i^x = -\omega_Z f_i^y \tag{S25c}$$

$$\dot{f}_i^y = \omega_Z f_i^x - \Omega_i S_z f_i^z \tag{S25d}$$

$$\dot{f}_i^z = \Omega_i S_z f_i^y. \tag{S25e}$$

Here $S_z$ is the component of the Stokes vector along the cavity axis, which is given in terms of $\mathcal{H}$ and $\mathcal{V}$ in Eq. S5.

While Equations S25 are exact, evaluating the exact time evolution including atom-light correlations is non-trivial. As a lowest-order approximation, we employ a mean-field treatment, calculating the approximate time-evolution of the expectation values $\langle\mathcal{V}\rangle, \langle\mathcal{H}\rangle$, and $\langle\mathbf{f}_i\rangle$ by neglecting atom-field correlations on the right-hand side of Eqs. S25.

We numerically solve Eqs. S25 in the mean-field approximation to obtain Fig. 2c in the main text, using the measurement of the vector light shift $\Omega(x)$ and the initial atomic state as inputs. The drive-cavity detuning $\delta_c = -2\pi \times 0.875$ MHz is fit by eye to match the data qualitatively and agrees within error with the value set during the experiment, $\delta_c = -2\pi \times 1.1(3)$ MHz. The drive strength $\varepsilon = 2\pi \times 95$ MHz used in the simulation corresponds to $\bar{n} = 12 \times 10^3$ intracavity photons (Eq. S16), consistent with the value $\bar{n} = 9(2) \times 10^3$ inferred from the cavity transmission.

Our simulation accounts for two different dissipation mechanisms that affect the coherence of the spin-exchange oscillations, namely, thermal broadening and cavity decay. These contributions are examined in detail in Fig. S1, where part (a) shows the model and data from Fig. 2 of the main text in terms of local magnetization $F_z \equiv \rho\langle f^z\rangle$, where $\langle f^z\rangle$ denotes local spin polarization and $\rho$ denotes local density. At fixed longitudinal position $x_i$, thermal

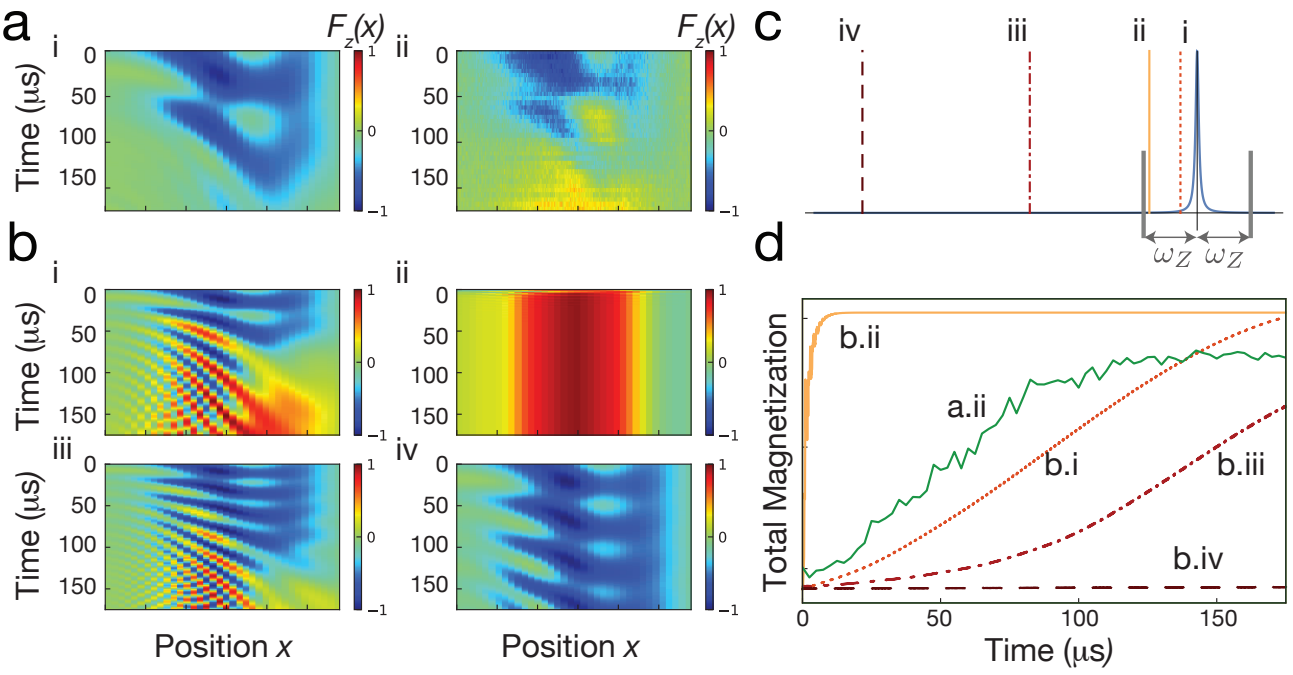


FIG. S1: **Effect of thermal broadening and supperradiant decay on the unitary dynamics.** (a) The model including thermal broadening (i) washes out the oscillations as in the experimental data (ii) compared to the zero-temperature model at the same detuning $\delta_- = 2\pi \times 1.93$ MHz (b.i), but artificially suppresses the relaxation rate compared to the data and the zero-temperature model (b.i). (b) The zero-temperature model shows rapid relaxation near the Raman resonance $\delta_- = 2\pi \times .30$ (ii) and slower relaxation at larger detunings $\delta_- = -2\pi \times 5.95, -2\pi \times 14.7$ MHz (iii, iv). (c) Schematic of drive detunings with respect to cavity and Raman resonances. (d) The total magnetization $\sum_x F_z(x)$ over the cloud is plotted vs time. Green curve corresponds to the data in (a)ii; solid orange-dashed burgundy curves correspond to calculated dynamics in (b)i-iv at the drive frequencies indicated by the lines in (c).

broadening results in a range of radial couplings $\Omega_i(r)$. The distribution of radial couplings is averaged over in our data (Fig. S1a.ii). To incorporate the effect of thermal broadening in the simulated dynamics, we average the dynamics over a Boltzmann distribution of atoms in the trap, assuming a Gaussian cloud of atoms in a three-dimensional harmonic well at each lattice site. The oscillations are washed out in a thermal cloud (Fig. S1a.i) compared to the dynamics at zero temperature (S1b.i) with all other parameters held fixed. The second mechanism is superradiant decay due to loss of cavity photons, which manifests as a spin relaxation rate towards either $m_f = \pm 1$, depending on the Raman detunings $\delta_\pm$. In Fig. S1b.i-iv, we plot the zero-temperature dynamics at detunings $\delta_- = 2\pi \times 1.93, 2\pi \times .30, -2\pi \times 5.95, -2\pi \times 14.7$ MHz (Fig. S1c) at fixed intracavity photon number. The relaxation rate is highest near the Raman resonance $\delta_- = 0$, but is suppressed for larger detunings, as summarized in Fig. S1d showing the total magnetization $\sum_x F_z(x)$ vs time.

Compared with the zero-temperature models and with our experimental data, the model including thermal broadening (Fig. S1a.i) shows a reduced relaxation rate. We attribute this to the fact that the static inhomogeneous couplings assumed in the model can lead to the formation of a dark state, which would decohere in the actual experiment due to atomic motion. Nevertheless, the key features of our data are well captured by the combination of these two models.

### C. Spin Mixing Dynamics

Here we derive the short-time equations of motion for the spin-mixing dynamics in the limit where atoms are uniformly coupled to the cavity mode, applying a mean-field treatment. We show that the results are equivalent to the well known mean-field treatments of spin-mixing in spinor Bose-Einstein condensates [4].

To model the spin mixing dynamics, we use a three-mode Schwinger boson representation for the collective spin $\mathbf{F}$ of the atomic ensemble:

$$F^+ = \sqrt{2}\left(a^\dagger c + c^\dagger b\right) = \left(F^-\right)^\dagger \tag{S26a}$$

$$F_z = a^\dagger a - b^\dagger b. \tag{S26b}$$

We obtain a Hamiltonian similar in form to a degenerate parametric oscillator with pump mode $c$ ($m_f = 0$) and side modes $a, b$ ($m_f = \pm 1$):

$$H_{\text{eff}} = 2\chi\left[c^\dagger c^\dagger ab + a^\dagger b^\dagger cc + a^\dagger a(1 + c^\dagger c) + c^\dagger c(1 + b^\dagger b)\right] + ha^\dagger a - hb^\dagger b + q(a^\dagger a + b^\dagger b), \tag{S27}$$

where $\chi = \chi^+ + \chi^-$, $h = \chi^+ - \chi^-$, and $q$ represents the quadratic Zeeman shift. Then, by treating the pump mode classically, $\hat{c} \to ce^{i\phi}$ and $\hat{c}^\dagger \to ce^{-i\phi}$ we obtain a quadratic Hamiltonian in the side mode operators $a, b$:

$$H_{\text{eff}} = 2\chi\left[c^2 e^{-2i\phi} ab + c^2 e^{2i\phi} a^\dagger b^\dagger + a^\dagger a(1 + c^2) + c^2(1 + b^\dagger b)\right] + ha^\dagger a - hb^\dagger b + q(a^\dagger a + b^\dagger b) \tag{S28}$$

We can conceptually simplify this further by introducing the bilinears

$$K_z = (a^\dagger a + b^\dagger b + 1)/2 \tag{S29a}$$

$$K^+ = a^\dagger b^\dagger = (K^-)^\dagger \tag{S29b}$$

where $2K_z - 1 = N_s$ is the total side-mode population and $K^\pm$ are 'pair-creation / annihilation' operators. The operators $\{K_z, K^\pm\}$ form a closed SU(1, 1) algebra [5–7]:

$$[K_z, K^\pm] = \pm K^\pm \tag{S30a}$$

$$[K^+, K^-] = -2K_z \tag{S30b}$$

The magnetization $F_z$ commutes with all of the operators $K^\pm, K_z$, so we can simply treat it as a constant $c$-number.

The group SU(1, 1) is very similar to the more familiar group SU(2). In fact, the only difference is the minus sign in the second row of Eq. (S30b). While SU(2) generates rotations in 3-dimensional Euclidean space, the group SU(1, 1) generates rotations and boosts in (2+1)-dimensional Minkowski space. In terms of $\mathbf{K}$, we can write the Hamiltonian as:

$$H_{\text{eff}} = \mathbf{M} \cdot \mathbf{K} \tag{S31}$$

where $K_x = (K^+ + K^-)/2$, $K_y = (K^+ - K^-)/2i$, and

$$\mathbf{M} = \langle 4c^2\chi \cos 2\phi, -4c^2\chi \sin 2\phi, \chi(2 + 4c^2) + 2q\rangle \tag{S32}$$

and where we have dropped an overall constant term $(\chi + h)F_z - \chi - q$.

We solve for the motion of the system assuming that the pump field is static (i.e. $c, \phi$ are time-independent). By performing a rotation in the $x-y$ plane we can always pick a coordinate system for which $\phi = 0$. Then our equations of motion are:

$$\frac{d}{dt}\begin{bmatrix} K_x \\ K_y \\ K_z \end{bmatrix} = \begin{bmatrix} 0 & -M_z & 0 \\ M_z & 0 & M_x \\ 0 & M_x & 0 \end{bmatrix}\begin{bmatrix} K_x \\ K_y \\ K_z \end{bmatrix} \tag{S33}$$

whose eigenvalues are 0 and $\pm\lambda = \pm\sqrt{M_x^2 - M_z^2}$, with $M_x = 4c^2\chi, M_z = \chi(2 + 4c^2) + 2q$. For $|M_z| < |M_x|$, the eigenvalue $\lambda$ is real and positive, resulting in the dynamical instability that we observe in our experiment. In terms of the net quadratic Zeeman shift $\tilde{q} = q + \chi$ and the number of "pump" atoms $c^2 \sim N_0$ in the $m = 0$ mode, the condition for instability is,

$$\left|1 + \frac{\tilde{q}}{2N_0\chi}\right| < 1 \tag{S34}$$

which is satisfied when $\tilde{q}$ and $\chi$ have opposite signs and the collective interaction strength $4N_0|\chi|$ exceeds the quadratic Zeeman shift. These are the same conditions for instability found for spin-mixing dynamics in spinor BECs.

To compute the time-dependent expectation value and standard deviation of $N_s(t)$, we assume that the system starts in a number state $|n_a, n_b, n_c\rangle$. We then obtain:

$$\langle N_s(t)\rangle = \alpha^2\left(N_s(0) + 1\right)\left(\cosh\lambda t - 1\right) + N_s(0) \tag{S35}$$

and

$$\Delta N_s(t) = \sqrt{\langle N_s^2(t)\rangle - \langle N_s(t)\rangle^2} = \left(N_s(0) + 1\right)\sqrt{\alpha^2\left[(\alpha^2 - 1)(\cosh\lambda t - 1)^2 + \sinh^2\lambda t\right]/2} \tag{S36}$$

where

$$\lambda = 2\sqrt{-\tilde{q}(\tilde{q} + 4c^2\chi)}, \tag{S37}$$

$$\alpha = \frac{4c^2|\chi|}{\lambda}. \tag{S38}$$

Although these equations of motion are applicable for perfectly uniform couplings $\Omega(x)$, accounting to lowest order for the non-uniformity of the couplings shows that the growth rate scales as $\xi_{\mathrm{rms}} = \sqrt{\sum_i \xi_i^2}$. We account for this effect in the main text by plotting the growth in side-mode population in Fig. 4 as a function of $\sqrt{\langle\Omega^2\rangle} = \Omega\xi_{\mathrm{rms}}$.

## II. EXPERIMENTAL METHODS

### A. Optical Cavity and Trapped Atoms

Our optical cavity has a near-concentric geometry with a maximum length $L_0 = 5$ cm. The precise length, as well as the mirror alignment, are fine-tuned with piezoelectric positioning stages. Our experiments were conducted at a cavity length $L = L_0 - 80$ $\mu$m, which results in a mode waist of $w_{780} = 16$ $\mu$m for the 780-nm drive field. The mirrors are additionally coated for 1560-nm light that is used to trap the atoms in one-dimensional lattice, with transverse confinement set by the waist $w_{1560} = \sqrt{2}w_{780}$. A typical trap depth during the experiment is $h \times 20$ MHz at the center of the cavity. The atomic cloud has an RMS width of 5 $\mu$m in the radial direction, is approximately 500 $\mu$m in length, and is centered about one Rayleigh length from cavity center.

### B. State Preparation and Detection

We provide here further details about the experimental sequence, including the state-sensitive imaging used to obtain measurements of the population in the three different Zeeman states. The atoms are loaded into the 1560-nm lattice from a 3D MOT, then placed in $|f = 1, m_f = -1\rangle$ by optical pumping into $|2, -2\rangle$ on the D1 line followed by an adiabatic microwave sweep. Additional microwave sweeps or optical Raman pulses are used to prepare the initial

Zeeman states for the subsequent quench dynamics. For the quench dynamics of Figs. 2 and 3 [or Fig. 4] in the main text, we apply a magnetic field $B_z = 4.0$ G [or $B_z = 1.0$ G], which adds to an ambient field $B_x = 0.52$ G, $B_y = -0.14$ G (axes as depicted in Fig. 1 of the main text). After the quench dynamics in the $f = 1$ hyperfine manifold, we detect the $|1,-1\rangle$ atoms by performing an adiabatic sweep on the $|1,-1\rangle \rightarrow |2,-2\rangle$ transition in a 4 G magnetic field and imaging on the cycling transition. We then detect the $|1,1\rangle$ atoms by performing a microwave sweep on the $|1,1\rangle \rightarrow |2,2\rangle$ transition and imaging on the cycling transition. Finally, we image the remaining atoms in $|1,0\rangle$ by adding repumping light.

### C. Measurement of Cavity Coupling

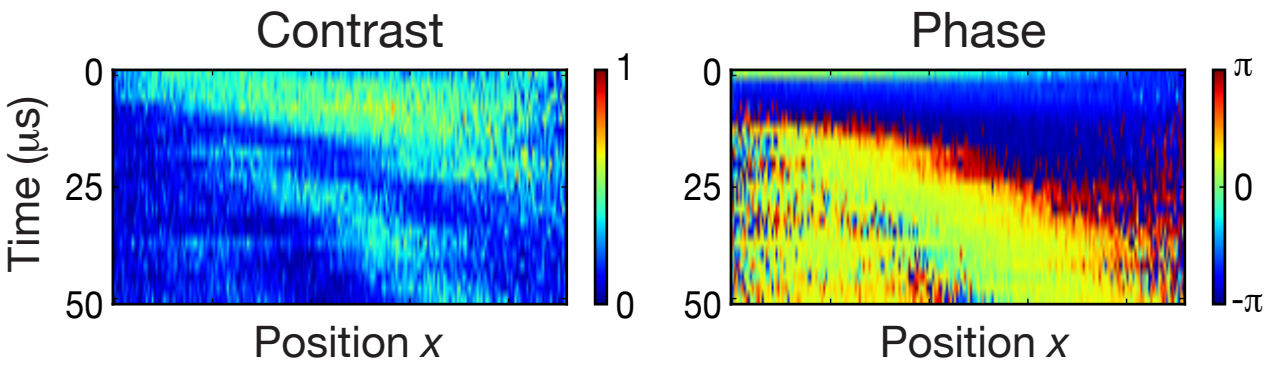


FIG. S2: Contrast and phase of the magnetization from the Ramsey measurement of the vector light shift. We measure the two quadratures $f_i^z(0), f_i^z(\pi/2)$ as a function of time, and can thus extract the local phase $\mathrm{Arg}(f_i^z(0) + i f_i^z(\pi/2))$ and contrast $\sqrt{(f_i^z(0))^2 + (f_i^z(\pi/2))^2}$.

We measured the vector light shift $\Omega(x)$ (Fig. 2b in the main text) by performing Ramsey spectroscopy in the $f = 1$ hyperfine manifold. After initializing the atoms in $|1,-1\rangle$ with respect to a magnetic bias field along the cavity axis, we first apply a Raman $\pi/2$ pulse that rotates the Zeeman spin into the $f_x, f_y$-plane. We then drive the cavity with a variable-length pulse of circularly polarized light that modifies the Larmor precession rate, before performing a second $\pi/2$ pulse and reading out the local magnetization $f_i^z$. Fig. S2 shows the contrast and phase of the Ramsey fringe as a function of the duration of the light pulse (Fig. S2). In the ideal case where the light shift $\Omega$ depends only on the position $x_i$, the magnetization would simply evolve as $f_i^z(t)/f_i = e^{-i\bar{n}\Omega_i t}$. However, our data shows a decaying contrast due to inhomogeneous broadening caused by a thermal distribution of radial couplings $P(\Omega_i(r))$ at a given position $x_i$ in the trap.

To model the Ramsey fringe, we assume that the atoms are in a two-dimensional harmonic trap with a radial distribution $P(r) = \frac{1}{\pi\rho w^2} e^{-r^2/\rho w^2}$, where $w = 16$ $\mu$m is the waist of the cavity mode for the 780-nm drive field, and $\rho$ is the local ratio of temperature to trap depth. We parameterize the vector light shift $\Omega_i(r) \approx (-1 + 2r^2/w^2)\Omega_i$ in terms of the magnitude $\Omega_i$ of the light shift on cavity axis ($r = 0$) for an atom in a lattice site at position $x_i$, averaged over the fast axial motion within the lattice site. We expect the magnetization at position $x_i$ to evolve as

$$\frac{f_i^z}{f_i}(t) = \int_0^{\Omega_i} P(\Omega_i(r)) e^{-i\bar{n}\Omega_i(r)t} d\Omega_i(r) = \int_0^1 \frac{1}{2\rho\Phi_i} \Phi_i^{1/2\rho} e^{-i\bar{n}\Phi_i(\tau-\tau_0)} d\Phi_i, \tag{S39}$$

where $\tau = \Omega_i t$, $\tau_0$ allows for an initial phase, and $0 \leq \Phi_i \equiv \Omega_i(r)/\Omega_i \leq 1$ is the local probe coupling in units of $\Omega_i$. Fitting Eq. S39 to the data at $x_i$ yields a value for $\bar{n}\Omega_i$, and we divide by the intracavity photon number $\bar{n}$ to obtain $\Omega(x_i) \equiv \Omega_i$.

### D. Extracting the Interaction Strength from Flip-Flop Measurements

To measure the strength and sign of the couplings $\chi_{ij}$, we first use a pair of Raman beams to prepare a region (A) of the atoms along $\hat{F}_x$ and another region $B$ along $\hat{F}_y$. In particular, after initializing all atoms in the $|m_f = -1\rangle$ state, we use a focused Raman beam to apply a local $\pi/2$ rotation to only the atoms in region (A). A second Raman

beam, phase-shifted by $\pi/2$ relative to the first beam, then addresses all atoms to apply a global $\pi/2$ rotation to the entire cloud. We then turn on photon-mediated interactions. In addition to coherent four-photon processes that cause each spin to precess about the mean field of the other spins, dissipative two-photon processes cause the spins to drift toward $m_f = \pm 1$, leading to a bias in the total magnetization. We extract both the mean interaction rate and mean decay rate by analyzing the sums and differences of the magnetization signals in the (A) and (B) regions.

To analyze the mean-field flip-flop dynamics, we first write the Hamiltonian and Lindblad operators of Eqs. S21 and S23 explicitly in terms of the local magnetization $\mathbf{F}_n \equiv \mathbf{F}(x_n)$:

$$H = 2\chi \sum_{n,m} \xi_n \xi_m \left(F_n^x F_m^x + F_n^y F_m^y\right) + \sum_n h_n F_n^z, \tag{S40a}$$

$$L_\pm = \sqrt{\gamma_\pm} \sum_n \xi_n F_n^\pm. \tag{S40b}$$

The indices $n, m$ label discrete regions in the 1-dimensional image obtained after summing over the transverse dimension of the cloud. Each region $n$ corresponds to a sum over many individual atoms, e.g.:

$$\mathbf{F}_n = \sum_{i \in n} \mathbf{f}_i, \tag{S41}$$

where we have assumed that the cavity couplings $\Omega(x)$ are approximately constant over the sites within each region. This coarse-graining over individual atoms justifies a classical calculation of the time evolution, where we approximate the $10^3 - 10^4$ uniformly polarized quantum spins in each analysis region as a single classical spin and neglect quantum correlations.

At short times, the classical spin model predicts the average magnetization $F_n^z$ in region $n$ to grow linearly in time at a rate dependent on the initial spin texture:

$$\frac{d}{dt} F_n^z = 2\xi_n \left(\mathcal{F}^x F_n^y - \mathcal{F}^y F_n^x\right) \chi - \xi_n \left(\mathcal{F}^x F_n^x + \mathcal{F}^y F_n^y\right) \gamma \tag{S42}$$

where $\gamma = \gamma_- - \gamma_+$ and $\mathcal{F} = \sum_n \xi_n \mathbf{F}_n$ is the collective spin, weighted by the cavity couplings. By measuring the linear growth rates in two different regions $n, m$ we obtain a pair of linear equations:

$$\frac{d}{dt} \begin{bmatrix} F_n^z \\ F_m^z \end{bmatrix} = \mathcal{M} \begin{bmatrix} \chi \\ \gamma \end{bmatrix} \tag{S43}$$

where the matrix $\mathcal{M}$ depends on the initial orientations of the spins in the two regions. We obtain an estimate for the initial local spin polarization $\mathbf{F}_n$ using the known spatial dependence of the two Raman beams, and we use the measured vector light shift $\Omega(x)$ (main text, Fig. 2b) to estimate the weights $\xi_n$. Inverting the matrix $\mathcal{M}$ then gives an estimate of the interaction and decay rates $\chi, \gamma$.


[1] K. Hammerer, A. S. Sørensen, and E. S. Polzik, Reviews of Modern Physics **82**, 1041 (2010).
[2] J. Kohler, J. A. Gerber, E. Dowd, and D. M. Stamper-Kurn, Physical Review Letters **120**, 013601 (2018).
[3] F. Reiter and A. S. Sørensen, Physical Review A **85**, 032111 (2012).
[4] D. M. Stamper-Kurn and M. Ueda, Reviews of Modern Physics **85**, 1191 (2013).
[5] B. Yurke, S. L. McCall, and J. R. Klauder, Physical Review A **33**, 4033 (1986).
[6] K. Wodkiewicz and J. H. Eberly, J. Opt. Soc. Am. B **2**, 458 (1985).
[7] C. C. Gerry, Phys. Rev. A **31**, 2721 (1985).